

# 000 001 002 003 004 005 HAMSTER: HIERARCHICAL ACTION MODELS FOR 006 OPEN-WORLD ROBOT MANIPULATION 007 008 009

010 **Anonymous authors**  
 011 Paper under double-blind review  
 012  
 013  
 014  
 015  
 016  
 017  
 018  
 019  
 020  
 021  
 022  
 023  
 024  
 025  
 026  
 027  
 028  
 029  
 030  
 031

## ABSTRACT

032 Large models have shown strong open-world generalization to complex problems  
 033 in vision and language, but they have been relatively more difficult to deploy in  
 034 robotics. This challenge stems from several factors, the foremost of which is the  
 035 lack of scalable robotic training data since this requires expensive on-robot collection.  
 036 For scalable training, these models must show considerable transfer across  
 037 domains, to make use of cheaply available “off-domain” data such as videos,  
 038 hand-drawn sketches, or data from simulation. In this work, we posit that hierar-  
 039 chical vision-language-action models can be more effective at transferring behav-  
 040 ior across domains than standard monolithic vision-language-action models. In  
 041 particular, we study a class of hierarchical vision-language-action models, where  
 042 high-level vision-language models (VLMs) are trained on relatively cheap data to  
 043 produce semantically meaningful intermediate predictions such as 2D paths indi-  
 044 cating desired behavior. These predicted 2D paths serve as guidance for low-level  
 045 control policies that are 3D-aware and capable of precise manipulation. In this  
 046 work, we show that separating prediction into semantic high-level predictions, and  
 047 3D-aware low-level predictions allows such *hierarchical* VLA policies to transfer  
 048 across significant domain gaps, from simulation to the real world or across scenes  
 049 with widely varying visual appearance. Doing so allows for the usage of cheap,  
 050 abundant data sources beyond teleoperated on-robot data thereby enabling broad  
 051 semantic and visual generalization. We demonstrate how hierarchical architec-  
 052 tures trained on such cheap off-domain data can enable robotic manipulation with  
 053 semantic, visual, and geometric generalization through experiments in simulation  
 054 and the real world.

## 1 INTRODUCTION

055 Developing general robot manipulation policies has been notoriously difficult. With the advent of  
 056 large vision-language models (VLMs) that display compelling generalizations, there is an optimism  
 057 that similar techniques can be helpful for robotic manipulation. Several prior works (Team et al.,  
 058 2024; Kim et al., 2024; Gu et al., 2023) build open-world vision-language-action models (VLAs)  
 059 by finetuning off-the-shelf, pretrained VLMs. The recipe for training many of these VLA mod-  
 060 els has been to collect and curate a large-scale robotics-specific dataset, complete with images and  
 061 corresponding on-robot actions, and then finetune a VLM to directly produce actions (Kim et al.,  
 062 2024; Brohan et al., 2023a). Such VLAs have shown robustness on simple tasks and controlled  
 063 environmental variations. However, these models display limited generalization in terms of environ-  
 064 ment, object, task, and semantic variation. This issue could be attributed to the scarcity of diverse,  
 065 in-domain training data. The data needed to train these models is expensive since it requires end-  
 066 to-end image-action pairs that must all be collected directly on-robot. A solution for training VLA  
 067 models must be developed to bring down the cost of data collection or learn from easy-to-collect  
 068 “cheap” sources of data.

069 On the other hand, relatively “small” imitation learning models have shown impressive dexterity  
 070 and geometric robustness. Such models have demonstrated promise across a range of complex  
 071 tasks involving contact-rich manipulation and 3D reasoning, spanning domains from tabletop ma-  
 072 nipulation (Shridhar et al., 2023; Goyal et al., 2023) to fine dexterous manipulation (Zhao et al.,  
 073 2023). Trained on relatively small datasets, these models show local robustness and stable control  
 074 but typically lack semantic or visual generalization. They are often brittle to changes in the envi-

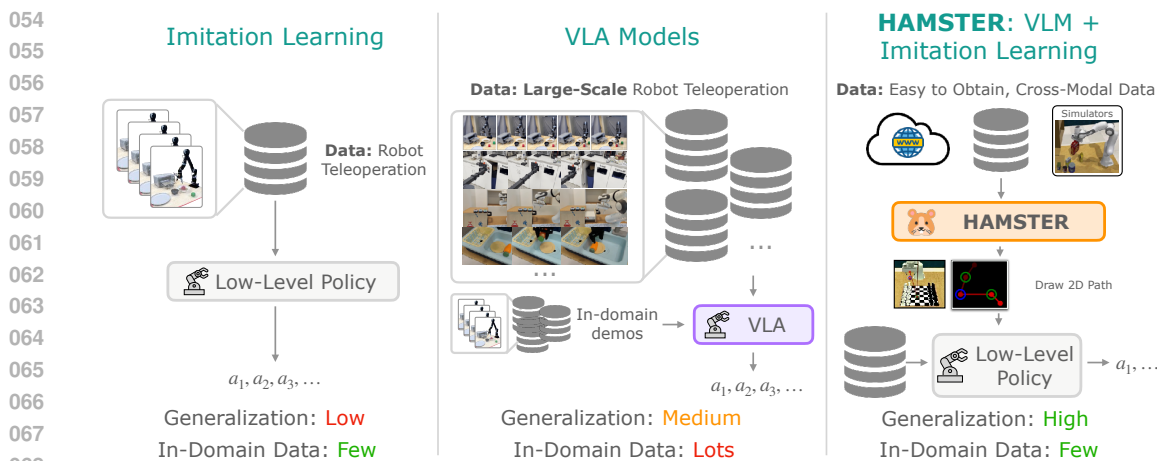


Figure 1: Overview of HAMSTER, VLAs and “smaller” imitation learning methods. HAMSTER’s hierarchical design results in better generalization with a small amount of in-domain data. HAMSTER is able to utilize cheap training sources such as videos or simulations for enhanced generalization.

environment, semantic description of the tasks, or changes in the objects being manipulated (Pumacay et al., 2024). This fragility can also be boiled down to scarce in-domain data collected on a robot. Reliable, generalizable robotic learning techniques must marry the generalization benefits of large VLMs, with the efficiency, local robustness and dexterity of small imitation learning policies, all while being able to train from abundant and cheap sources of data. In this work, we ask – can we design VLA models that train on relatively abundant and cheap data sources, showing broad visual and semantic generalization, while capturing the low-level geometric and 3D understanding displayed by small imitation learning models?

We propose that a hierarchical architecture for vision-language-actions models, HAMSTER (**H**ierarchical **A**ction **M**odels with **S**epa**T**Ed **P**ath **R**epresentations), can serve as an effective way to learn from abundant and cheap sources of data such as videos or simulation. We study a family of HAMSTERs, where finetuned VLMs are connected to low-level 3D policy learning methods via intermediate 2D path representations. Since these 2D paths can easily be obtained in abundance from data sources such as videos or simulations (either with point tracking, hand-sketching, or proprioceptive projection), these can be used to finetune the larger higher-level VLM in HAMSTER. These 2D paths can then serve as guidance for a low-level policy that operates on rich 3D and proprioceptive inputs, alleviating the burden of long-horizon planning and semantic reasoning, allowing low-level policies to focus on robustly generating precise, spatially-aware actions.

Representations similar to 2D paths has been explored in the robot learning literature (Gu et al., 2023), primarily as a technique for flexible task specification. However, the key hypothesis explored in this paper is distinct – we posit that using cheap data such as videos or simulation to finetune *hierarchical* path generating VLMs can enable a surprising degree of cross-domain transfer as compared to the direct transfer of monolithic vision-language-action models (Brohan et al., 2022; Kim et al., 2024). Here the focus is less on using paths as a scalable technique for task specification, and more on using hierarchy as a mechanism for robust cross-domain transfer across settings with considerable visual and semantic differences. Specifically, we find that VLMs trained to predict 2D path representation can transfer to the real world from simulations that look very different from the real world, or across real-world scenarios with widely varying appearance. Hence, the hierarchical design of HAMSTER provides a way to utilize cheaper, but perceptually varying sources of “off-domain” data (such as simulation or cross-embodiment data) to benefit real-world control policies.

The hierarchical design presented in HAMSTER can also offer additional advantages through the decoupling of VLM training and low-level action prediction. Specifically, since the higher-level VLM is predicting semantically meaningful trajectories from monocular RGB camera inputs, the lower-level control policies can operate from rich 3D and proprioceptive inputs. In doing so, HAMSTER inherits the semantic reasoning benefits of VLMs along with the 3D reasoning and spatial awareness benefits of 3D imitation learning policies (Goyal et al., 2024; Ke et al., 2024). Finally, since HAMSTER is built on both open-source VLMs and low-level policies, it can serve as a fully open-sourced enabler for the community-building vision-language-action models.

108    **2 RELATED WORK**

110    **LLMs and VLMs for robotics.** Early attempts in leveraging LLMs and VLMs for robotics are  
 111    through pretrained language (Jang et al., 2022; Shridhar et al., 2023; Singh et al., 2023) and vi-  
 112    sual (Shah & Kumar, 2021; Parisi et al., 2022; Nair et al., 2023; Ma et al., 2023) models. However,  
 113    these are not sufficient for complex semantic reasoning and generalization to the open world (Bro-  
 114    han et al., 2022; Zitkovich et al., 2023). Recent research has focused on directly leveraging open  
 115    world reasoning and generalization capability of LLMs and VLMs, by prompting or fine-tuning  
 116    them to, e.g., generate plans (Huang et al., 2022; 2023b; Lin et al., 2023; Liang et al., 2023; Singh  
 117    et al., 2023; Brohan et al., 2023b), construct value (Huang et al., 2023a) and reward functions (Kwon  
 118    et al., 2023; Sontakke et al., 2023; Yu et al., 2023; Ma et al., 2024; Wang et al., 2024). Our work is  
 119    more closely related to the literature on VLA models, summarized below.

120    **Monolithic VLA models as language-conditioned robot policies.** Monolithic VLA models have  
 121    been proposed to produce robot actions given task description and image observations directly (Bro-  
 122    han et al., 2022; Jiang et al., 2023; Zitkovich et al., 2023; Team et al., 2024; Kim et al., 2024;  
 123    Radosavovic et al., 2023). Monolithic VLA models are often constructed from VLMs (Liu et al.,  
 124    2024b; Bai et al., 2023; Driess et al., 2023; Lin et al., 2024), and are trained on large-scale robot  
 125    teleoperation data (Brohan et al., 2022; Collaboration et al., 2023; Khazatsky et al., 2024) to predict  
 126    actions as text or special tokens. However, due to the lack of coverage in existing robotics datasets,  
 127    they must be finetuned in-domain on expensive teleoperated data. The most relevant monolithic  
 128    VLA model is LLARVA (Niu et al., 2024), which predicts end-effector trajectories in addition to  
 129    robot actions. However, LLARVA does not use trajectory prediction to control the robot; rather, it  
 130    uses it as an auxiliary task to improve action prediction. Therefore, LLARVA still suffers from the  
 131    limitations of monolithic VLA models. In contrast, our work takes a hierarchical approach, drasti-  
 132    cally reducing the number of demonstrations needed for learning downstream tasks and the number  
 133    of VLM calls per episode. Moreover, our proposed hierarchical architecture enables training from  
 134    cheaper data sources while enabling considerable cross-domain transfer.

135    **VLMs for predicting intermediate representations** Our work bears connections to prior methods  
 136    using vision-language models for intermediate prediction. These methods can be categorized by the  
 137    choice of predicted representation:

138    *Point-based predictions:* A common intermediate prediction interface has been keypoint afford-  
 139    ances (Stone et al., 2023; Sundaresan et al., 2023; Nasiriany et al., 2024; Yuan et al., 2024). Some  
 140    examples include using open-vocabulary detectors (Minderer et al., 2022), iterative prompting of  
 141    VLMs (Nasiriany et al., 2024), or fine-tuning detectors to identify certain parts of an object by se-  
 142    mantics (Sundaresan et al., 2023). Perhaps most related, Yuan et al. (2024) finetunes a VLM to  
 143    predict objects of interest as well as free space for placing an object, and Liu et al. (2024a) propose  
 144    a mark-based visual prompting procedure to predict keypoint affordances as well as a fixed number  
 145    of waypoints. As opposed to these, our work finetunes a VLM model to not just predict points but  
 146    rather entire 2D paths, making it more broadly applicable across robotic tasks.

147    *Trajectory-based predictions:* The idea of using trajectory-based task specifications to condition  
 148    low-level policies was proposed in RT-trajectory (Gu et al., 2023), largely from the perspective  
 149    of flexible task specification. This work also briefly discusses the possibility of combining RT-  
 150    Trajectory with trajectory sketches generated from prompting a pre-trained vision language model.  
 151    Complementary to RT-Trajectory, the focus of this work is less on the use of trajectory sketches for  
 152    task specification, but rather on the abilities of a hierarchical VLA model to finetune the high-level  
 153    VLM on cheap and abundant sources. This could include training data such as videos or simu-  
 154    lation data, and show transfer to test scenarios of interest with considerable visual and semantic  
 155    variation. While RT-trajectory uses human effort or off-the-shelf pre-trained models to generate  
 156    trajectories, we show that finetuning VLM models on cheap data sources can generate more accu-  
 157    rate and generalizable trajectories (see Table. 2). Moreover, our instantiation of this architecture  
 158    enables the incorporation of rich 3D and proprioceptive information, as compared to monocular 2D  
 159    policies (Gu et al., 2023).

160    **Leveraging simulation data for training robot policies.** There has been extensive work on lever-  
 161    aging simulation for robot learning. Simulation data is popular in reinforcement learning (RL),  
 162    as RL on real robotic systems is often impractical due to high sample complexity and safety con-  
 163    cerns (Lee et al., 2020; Handa et al., 2023; Torne et al., 2024). Recently, simulation has been also

exploited to directly generate (Fishman et al., 2022) or bootstrap (Mandlekar et al., 2023) large-scale datasets for imitation learning, to reduce the amount of expensive robot teleoperation data needed. Our work takes a different approach - using simulation data to finetune a VLM, and showing that VLM is able to transfer the knowledge learned from simulation data to real robot systems, despite considerable visual differences. A related observation is recently made by (Yuan et al., 2024), but they use keypoint affordances as the interface between the VLM and the low-level policy as opposed to more general expressive 2D path representations.

169

### 170 3 BACKGROUND

171

**172 Imitation Learning via Supervised Learning:** The goal of imitation learning is to train a prob-  
 173 abilistic policy  $\pi_\theta(a | s, o, z)$  from an expert-provided dataset. This policy  $\pi_\theta$  outputs the prob-  
 174 ability of producing action  $a$  conditioned on proprioceptive states  $s$ , perceptual observations  $o$ ,  
 175 and language instructions  $z$  that specify the task. In the typical imitation learning setting, a  
 176 dataset of expert in-domain trajectories is provided, consisting of observation-action-language tu-  
 177 ples  $\mathcal{D} = \{(s_i, a_i, o_i, z_i)\}_{i=1}^N$ . This dataset can be utilized to learn the parameters of the policy  $\pi_\theta$ .  
 178 While  $\pi$  can take on a variety of architectures with various training objectives (Goyal et al., 2023; Ke  
 179 et al., 2024; Zhao et al., 2023; Chi et al., 2023), most imitation learning algorithms are trained via  
 180 supervised learning to maximize the objective:  $\mathbb{E}_{(s_i, a_i, o_i, z_i) \sim \mathcal{D}} [\log \pi_\theta(a_i | s_i, o_i, z_i)]$ . This core  
 181 objective can be modified with rich architectural choices such as 3D policy architectures (Goyal  
 182 et al., 2023; Ke et al., 2024) or more expressive policy distribution classes (Zhao et al., 2023; Chi  
 183 et al., 2023), but generalization to out-of-domain to settings with semantic or visual variations is still  
 184 challenging. We study how vision-language models can be used to aid the generalization of such  
 185 low-level imitation learning-based policies, discussed in Section 4.1.

186

**187 Vision Language Models:** Typical vision language models (VLMs) (Lin et al., 2024; Liu et al.,  
 188 2024b) are large transformers (Vaswani et al., 2023) that take vision & text tokens as input and  
 189 produce text responses. These models are pre-trained on large multimodal datasets (Zhu et al.,  
 190 2023; Byeon et al., 2022), and then finetuned on targeted high-quality datasets (Shen et al., 2021;  
 191 Lu et al., 2022). These models tokenize each modality into a shared space to produce a sequence of  
 192 output tokens corresponding to text or other output modalities. In this work, we assume access to  
 193 a pre-trained, text and image input VLM (Lin et al., 2024; Liu et al., 2024b), that autoregressively  
 194 outputs a sequence of text tokens conditioned on an image and previous text tokens. These pretrained  
 195 VLMs can typically be finetuned using a supervised prediction loss that minimizes the negative log-  
 196 likelihood of the answer text tokens.

197

### 198 4 HAMSTER: HIERARCHICAL ACTION MODELS FOR ROBOTIC LEARNING

199

In this work, we examine how VLA models can be trained on relatively abundant data to demonstrate cross-domain transfer capabilities, as opposed to training on expensive image-action data collected on a robot. HAMSTER is a family of hierarchical action models designed for this purpose, exhibiting generalizable and robust manipulation. It consists of two interconnected models: first, a higher-level VLM that is fine-tuned on large-scale, cross-modal data to produce intermediate guidance (detailed in Section 4.1), and second, a low-level policy that produces actions conditioned on the VLM’s predicted guidance (detailed in Section 4.2). The finetuned VLM and the low-level policy communicate using a 2D path representation. Figure 2 provides an overview of HAMSTER’s design. Crucially, we study the ability of such a hierarchical design to enable training on cheap, abundantly available data such as simulation and videos.

200

**201 Problem Definition.** Rather than operating in the pure imitation learning setting as described  
 202 in Section 3, we study a scenario where cross-domain data is utilized to train VLA models.  
 203 While the typical imitation learning setting uses a dataset of optimal in-domain, on-robot tuples  
 204  $\mathcal{D} = \{(s_t, a_t, o_t, z_t)\}_{t=1}^N$  to learn a near-optimal policy  $\pi_\theta$ , in this setting we additionally assume  
 205 access to a much larger dataset(s) of “off-domain” approximately optimal data  $\mathcal{D}_{\text{off}} = \{(o_i^o, z_i^o)\}_{i=1}^M$ ,  
 206 where  $M \gg N$ , such as video or simulation data. This “off-domain” data  $\mathcal{D}_{\text{off}}$  is different from  
 207 in-domain data  $\mathcal{D}$  in several important ways: 1) Off-domain perceptual observations  $o_i^o$  may be con-  
 208 siderably different than in-domain perceptual observations  $o_i$ , even when the underlying physical  
 209 state of the system is similar An illustrative example of this is the marked difference between simu-

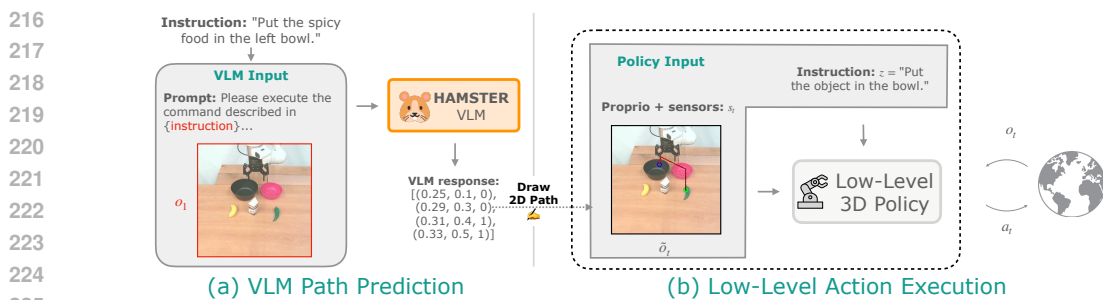


Figure 2: Depiction of HAMSTER’s execution. The high-level VLM is called once to generate the 2D path. The low-level policy is conditioned on the 2D path and interacts with the environment sequentially to execute low-level actions. The path predicted by the VLM enhances the low-level policy generalization capability.

lation and real-world scene appearance (see Figure. 5). 2) The underlying physical dynamics of the system can be potentially different, i.e the transition dynamics  $\mathbb{P}(s'|s, a)$  between states  $s'$ ,  $s$  may be different between off-domain sources such as video or simulation than the test-time deployment setting. While the dynamics may show level differences, we assume the higher-level coarse strategies to solve the task remain invariant. 3) Off-domain data may not have access directly to actions  $a$  or proprioception  $p$ , for instance in video based datasets. This poses challenges to directly applying the standard imitation learning paradigm for these datasets.

The goal is to leverage the combination of a small amount of “expensive” in-domain data  $\mathcal{D}$  and a large amount of relatively “cheap” off-domain data  $\mathcal{D}_{\text{off}}$  to obtain a generalizable policy  $\pi_\theta$  that can be successfully deployed over various initial conditions, task variations, and visual variations in the in-domain robot environment. Without additional assumptions, this problem is arduous due to the lack of alignment between the in-domain and off-domain settings. In this work, we assume access to an intermediate *path-labeler*  $p_i = h(o_i, z_i)$  at training time, that accepts an observation  $o_i$  and a language instruction  $z_i$  from either the off-domain or in-domain datasets, to produce an intermediate path label  $p_i$  that indicates *how* to optimally perform the task  $z_i$  from the observation  $o_i$ . In this work, we choose this intermediate path label  $p_i$  to be a sequence of points, a 2D path, on the image that indicates coarse end-effector motion to solve the designated task. This path-labeler at training time can come from different sources – a projection of known proprioception if available, human-drawn trajectory annotations on images, point-tracked end-effector or hand positions from video, and so on. Applying such a path labeler to the off-domain dataset yields  $\tilde{\mathcal{D}}_{\text{off}} = \{(o_i^o, z_i^o, p_i^o)\}_{i=1}^M$ .

#### 4.1 HAMSTER’s VLM FOR PRODUCING 2D PATHS TRAINED FROM OFF-DOMAIN DATA

The first stage of building a HAMSTER VLA model is finetuning a high-level VLM that predicts coarse 2D paths  $p$  given a language instruction  $z$  and observation  $o$ . This path represents the approximate trajectory of the robot end-effector on the input camera image. It also contains information about the gripper state (where to open the gripper and where to close it) as subsequently explained.

Although, conceptually, any VLM can be used to predict such a 2D path by casting an appropriate prompt, we find that standard pre-trained VLMs struggle with predicting such a path in a zero-shot manner (see Table 2). Therefore, we finetune pre-trained VLMs on datasets that ground VLMs to robot scenes and path predictions collected from easier-to-obtain sources, i.e., internet visual-question-answering data, robot data from other modalities, and simulation data. The primary advantages of finetuning such a hierarchical VLM that produces intermediate representations  $\hat{l}_i$ , as opposed to directly producing actions  $a$  with a monolithic model (Kim et al., 2024; Zitkovich et al., 2023) are twofold: 1) the lack of actions in certain off-domain datasets (such as videos) makes it impossible to even train monolithic pixel-to-action models, 2) we find empirically that hierarchical VLMs producing intermediate cross-domain predictions generalize more effectively than monolithic VLA models.

**Finetuning Objective and Datasets** We use VILA-1.5-13b (Lin et al., 2024), a 13-billion-parameter vision language model trained on interleaved image-text datasets and video captioning data, as our base VLM. We then curate a multi-domain dataset to finetune this model for effective 2D path prediction. Predicting the 2D path of the end-effector requires understanding *what* objects

270 to manipulate in a given task in terms of their pixel positions, but also reasoning about *how* a robot  
 271 should perform the task. To enable this understanding, we collate a diverse off-domain dataset  $\mathcal{D}_{\text{off}}$   
 272 from a wide range of modalities, including real-world data, visual question-answering data, and  
 273 simulation data. Importantly, *none* of this off-domain data used to train the VLM comes from the  
 274 deployment environment, thereby emphasizing generalizability. However, as outlined in Section 4.2,  
 275 the predictions of this trained VLM are used to guide a low-level policy at inference time.

276 We assemble a dataset  $\tilde{\mathcal{D}}_{\text{off}} = \{(o_i^o, z_i^o, p_i^o)\}_{i=1}^M$  of image inputs  $o_i^o$ , language prompts  $z_i^o$ , and path  
 277 labels  $p_i^o$  consisting of three types of data: (1) pixel point prediction tasks (*what*); (2) simulated  
 278 robotics tasks (*what and how*); (3) a real robot dataset consisting of trajectories (*what and how*). We  
 279 detail each dataset below; see Figure 6 for visualization of each dataset’s prompts and labels.  
 280

281 **Pixel Point Prediction.** For pixel point prediction, we use the dataset released by Robo-  
 282 Point (Yuan et al., 2024) with 1.4 million VQA tasks, with most answers represented as a  
 283 list of 2D points corresponding to locations on the image. A sample consists of a prompt  
 284  $z^o$  like Find all instances of cushions, an input image  $o^o$  and labels  $p^o$  like  
 285  $[(0.25, 0.11), (0.22, 0.19), (0.53, 0.23)]$ .<sup>1</sup> This dataset consists of data automatically generated in  
 286 simulation and collected from existing real-world datasets; its diversity and tasks enable the HAM-  
 287 STER VLM to reason about pixel-object relationships across diverse scenes while retaining its se-  
 288 mantic generalization capabilities.

289 **Robot Simulation Data.** We additionally generate a dataset of simulated robotics tasks from RL-  
 290 Bench (James et al., 2020), a simulator of a Franka robot performing tabletop manipulation for a  
 291 wide array of both prehensile and non-prehensile tasks. We use the simulator’s built-in planning al-  
 292 gorithms to automatically generate successful manipulation trajectories and construct ground-truth  
 293 2D path labels  $p^o$ . Each trajectory contains a sequence of 3D coordinates of the robot’s gripper  
 294 in world space, as well as whether the gripper is open or closed at a given time step. We use  
 295 known camera intrinsics and extrinsics to project these points on the front image and construct  
 296 labels  $p^o = [(x_{\text{image}}, y_{\text{image}}, \text{gripper\_open}), \dots]$  where  $x_{\text{image}}, y_{\text{image}} \in [0, 1]$  are relative pixel  
 297 locations of the end effector’s position on the image. The front camera image of the initial state  
 298 forms the image input  $o^o$  and the prompt  $z^o$  for the VLM is to provide a sequence of points denot-  
 299 ing the trajectory of the robot gripper to achieve the given instruction (see Figure 2). We generate  
 300 1000 episodes for each of 79 robot manipulation tasks in RLBench, each episode with  $\sim 4$  language  
 301 instructions, for a total of  $\sim 300$ k  $(o^o, z^o, p^o)$  tuples for  $\tilde{\mathcal{D}}_{\text{off}}$ .

302 **Real Robot Data.** Using real robot data allows us to ensure the VLM can reason about objects  
 303 and robot gripper paths when conditioned on scenes, including real robot arms. We use existing,  
 304 online robot datasets *not from the deployment environment* to enable this VLM ability. We source  
 305 10k trajectories from the Bridge dataset (Walke et al., 2023; Collaboration et al., 2023) consisting of  
 306 a WidowX arm performing manipulation tasks and 45k trajectories from DROID (Khazatsky et al.,  
 307 2024). For both datasets, we use the given end-effector trajectories and given (or estimated) camera  
 308 matrices to convert robot gripper trajectories to 2D paths  $p^o$ . We use a camera image from the first  
 309 timestep of each robot trajectory as  $o^o$  and a similar text prompt  $z^o$  as the simulation dataset. Note  
 310 that we essentially utilize the robot data as video data, where the end effector is tracked over time.  
 311 In principle, this could be done with any number of point-tracking methods (Doersch et al., 2023)  
 312 on raw video as well, with no action or proprioceptive labels.

313 **VLM Training.** We finetune the HAMSTER VLM on all three datasets by randomly sampling  
 314 from all samples in the entire dataset with equal weight. One problem with directly training on  
 315 the path labels  $p^o$  is that many paths may be extremely long, e.g., exceeding one hundred points.  
 316 Since we want the HAMSTER VLM to reason at a *high level* instead of on the same scale as the  
 317 low-level control policy. Therefore, we simplify the paths  $p^o$  with the Ramer-Douglas-Peucker  
 318 algorithm (Ramer, 1972; Douglas & Peucker, 1973) that reduces curves composed of line segments  
 319 to similar curves composed of fewer points. We train with the standardized supervised prediction  
 320 loss to maximize the log-likelihood of the language labels  $p^o \mathbb{E}_{(o_i^o, z_i^o, p_i^o) \sim \tilde{\mathcal{D}}_{\text{off}}} \log \text{VLM}(p_i^o | z_i^o, o_i^o)$ .  
 321

322  
 323 <sup>1</sup>Note that this is not a temporally ordered path, but rather simply a set of unordered points of interest in an  
 324 image. We overload notation here for the sake of notational convenience.

324    4.2 PATH GUIDED LOW-LEVEL POLICY LEARNING  
 325

326    After training the HAMSTER VLM to predict paths, we train a low-level policy to utilize these paths  
 327    to predict actions. While a low-level control policy *can* learn to solve the task without access to 2D  
 328    path predictions, providing it with 2D paths can make the task easier. The paths allow the low-level  
 329    policy to forgo long-horizon and semantic reasoning and focus on local and geometric predictions to  
 330    produce low-level actions. As we find empirically (see Figure. 3), 2D paths allow for considerably  
 331    improved visual and semantic generalization of low-level policies. We train low-level policies based  
 332    on rich 3-D perceptual information, available at test time on a robotic platform with standard depth  
 333    cameras. Then the question becomes—how do we incorporate 2D path information  $\hat{p}$  produced by  
 334    the VLM in Section 4.1 onto the 3D inputs to enable generalizable robot manipulation?

335    **Conditioning on Paths.** We convert 2D paths of the form  $p = \{(x_i, y_i, \text{gripper\_open})\}_{t=1}^L$   
 336    into a format that is easy to incorporate into any language ( $z$ ), proprioception ( $s$ ), and image ( $o$ )  
 337    conditioned policy  $\pi_\theta(a | s, o, z)$ . While one could concatenate the path with the proprioception or  
 338    language input, paths are of varied lengths, and this could prevent the integration of such paths into  
 339    existing policy architectures that cannot take in varied proprioceptive or language inputs. Instead, we  
 340    directly draw the 2D path points onto the image input to the policy, which is not only generalizable  
 341    across policy architectures but also may provide easier-to-follow path guidance as the policy does  
 342    not have to learn how to associate path points with their corresponding image locations (Gu et al.,  
 343    2023). During training, we use oracle paths constructed by projecting end-effector points to the  
 344    camera plane as described for simulation and real robot data in Section 4.1.

345    Formally, we iterate through each trajectory  $\tau_i = \{s_i^t, a_i^t, o_i^t, z_i\}_{t=1}^T$  on the in-domain dataset  $\mathcal{D}$  to  
 346    obtain the path  $p_i$ . Gu et al. (2023) proposed using colored trajectories to guide a policy’s actions,  
 347    and we largely follow their method of coloring trajectories to indicate gripper status and progression  
 348    through time. These paths are drawn onto all images in the trajectory  $o_i^1 \dots o_i^T$  by drawing points  
 349    at each  $(x, y)$  and connecting them with line segments to obtain  $\{\tilde{o}_i^t\}_{t=1}^T$ . We use a color gradient  
 350    to indicate progression through time (see Figure 2(b) for an example). We plot circles for change  
 351    in gripper status: e.g., green for closing the gripper and blue for opening. This constructs the final  
 352    in-domain path-labeled dataset  $\mathcal{D}_{\text{path}} = \{(s_i, a_i, \tilde{o}_i, z_i)\}_{i=1}^N$ .

353    **Imitation Learning.** Finally, we train a policy  $\pi_\theta(a | s, \tilde{o}, z)$  conditioned on proprioception and  
 354    other sensor information  $s$ , path-annotated image observations  $\tilde{o}$ , and a task language instruction  $z$   
 355    on  $\mathcal{D}_{\text{path}}$ . HAMSTER’s general path-conditioning framework allows for using arbitrary lower-level  
 356    control policies as they do not need to condition on the same inputs as the VLM. Therefore, we  
 357    train 3D low-level policies, such as RVT-2 (Goyal et al., 2024) and 3D-DA (Ke et al., 2024), for  
 358    low-level control. Here, we assume  $s$  includes additional sensor information (i.e., depth), which  
 359    3D-DA and RVT-2 utilize to construct point clouds and virtual camera renderings, respectively, for  
 360    more accurate control and data-efficient imitation learning. We directly train these policies, with  
 361    no necessary architectural changes,<sup>2</sup> with their supervised imitation learning objectives on  $\mathcal{D}_{\text{path}}$  to  
 362    maximize log-likelihoods of the dataset actions:  $\mathbb{E}_{(s_t, a_t, \tilde{o}_t, z_t) \sim \mathcal{D}_{\text{path}}} \log \pi_\theta(a | s_t, \tilde{o}_t, z_t)$ . For further  
 363    implementation details, see Appendix B.

364    **Online Evaluation** Standard VLA architectures query the VLM for every low-level action (Kim  
 365    et al., 2024; Brohan et al., 2023a), which can be very expensive with large VLMs—for example,  
 366    OpenVLA’s 7B param VLA only runs at 6Hz on an RTX 4090 (Kim et al., 2024). Instead, HAM-  
 367    STER’s hierarchical design allows us to query the VLM just once at the beginning of the episode  
 368    to generate a 2D path  $\hat{l}$  that we draw onto every subsequent image.<sup>3</sup> Therefore, HAMSTER can be  
 369    scaled to large VLM backbones without needing end-users to be concerned about inference speed.

370    5 EXPERIMENTAL EVALUATION  
 371

372    To test the hypotheses proposed in Section 4, we perform empirical evaluations in both simulation  
 373    and the real world. The experiments primarily aim to answer the following questions: (1) do hierar-  
 374    chical VLA models enable behavioral generalization to unseen scenarios? (2) do hierarchical VLA

375    <sup>2</sup>We ignore the language instruction for RVT-2 it is already encoded in the 2D path.

376    <sup>3</sup>HAMSTER is not inherently limited to being queried once per episode, but for simplicity and computa-  
 377    tional efficiency we query just once per episode in our experiments.

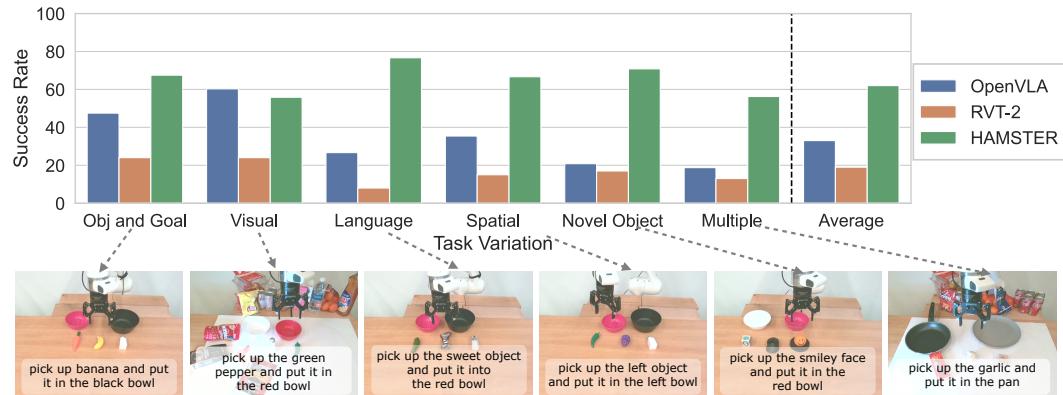


Figure 3: Depiction of quantitative real-world policy execution results on a real-world robot, evaluated across different axes of generalization. Across all generalization axes, HAMSTER outperforms monolithic VLAs and 3D imitation learning policies.

models show more effective cross-domain generalization than monolithic VLA models or low-level imitation learning methods? (3) is behavior learned by hierarchical VLA models robust to significant degrees of visual and semantic variations? (4) does including cross-domain data from settings like simulation really help with model generalization? (5) does explicitly finetuning the high-level VLM yield benefits in terms of spatial and semantic reasoning?

### 5.1 REAL WORLD EVALUATION ON TABLETOP MANIPULATION

Our real-world evaluation experiments aim to test the generalization capability of hierarchical VLA models across significant semantic and visual variations. In particular, we consider a variant of HAMSTER that uses a VLM (ViLA-1.5-13b) finetuned on the data mixture in Section 4.1 as the high-level predictor, with a 3-D policy architecture - RVT-2 (Goyal et al., 2024) as the choice of low-level policy, as described in Section 4.2. The low-level 3D policy is trained with 320 episodes collected via teleoperation directly on the table-top manipulation setup shown in Fig. 6. Importantly, the high-level VLM in HAMSTER is not finetuned on any in-domain data and is directly transferred only from the cheap data sources described in Section 4.1. This suggests that any generalization that the VLM sees does not result from in-domain training data rather than from cross-domain transfer.

*Baseline comparisons:* We compare HAMSTER to a state-of-the-art monolithic VLA, OpenVLA (Kim et al., 2024), as well as a non-VLM 3D imitation learning policy. For fair comparison, we finetune OpenVLA on the collected in-domain trajectory data described above, since OpenVLA showed poor zero-shot generalization to the testing domain. For the 3D imitation learning policy, we use RVT-2 (Goyal et al., 2024) as our baseline, as it is effective in learning robust policies with few demonstrations. The RVT-2 baseline is trained with the same teleoperation data used to train the low-level policy in HAMSTER but without the intermediate 2D path representation from HAMSTER’s VLM.

Figure 3 summarizes our real-world results. We compile results for multiple tasks, including ‘pick and place’, ‘push buttons’, and ‘knock down objects’. Similar to prior works (Kim et al., 2024), we test generalization across various axes, including: *Arrangement*: novel rearrangement of seen objects; *Visual*: visual generalization with pose changes in the target object and changes in table texture, lighting, and distractors; *Language*: semantic generalization with unseen language instructions to describe the task and target objects; *Novel Object*: testing scenarios with objects that are unseen in the training data; and lastly combinations of multiple of the above factors applied simultaneously. In total, we do 132 tests across all the models.

We find that HAMSTER is able to outperform monolithic VLA models as well as 3D imitation learning methods. This is significant because this improved performance is in the face of considerable visual and semantic changes in the test setting, showing the ability of HAMSTER to transfer much more effectively than monolithic VLA models or non-VLM base models. We refer readers to the supplementary website for additional details on the failure modes and evaluation conditions.

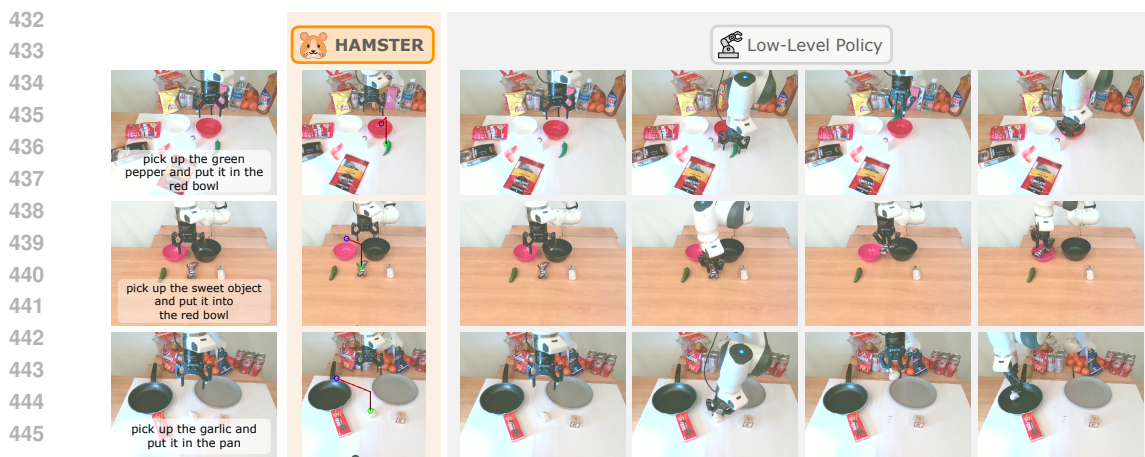


Figure 4: Examples of real-world executions of HAMSTER demonstrate its strong performance in novel complex scenes, achieved by leveraging the generalization capabilities of VLMs and the robust execution of low-level 3D policies.

	Avg.	no var	bac tex	cam pos	distractor	lig col	man obj col	man obj siz
3D-DA[ Ke et al.]	0.44	<b>0.53</b> ± 0.04	0.37 ± 0.07	<b>0.45</b> ± 0.38	0.28 ± 0.24	0.62 ± 0.30	0.55 ± 0.36	0.33 ± 0.21
HAMSTER (w 3D-DA)	<b>0.52</b>	0.48 ± 0.32	<b>0.46</b> ± 0.07	0.41 ± 0.11	<b>0.43</b> ± 0.10	<b>0.66</b> ± 0.20	<b>0.61</b> ± 0.10	<b>0.66</b> ± 0.25
	man obj tex	rec obj col	rec obj siz	rec obj tex	rlb and col	rlb var	tab col	tab tex
3D-DA[ Ke et al.]	<b>0.54</b> ± 0.18	0.3 ± 0.08	0.26 ± 0.16	0.45 ± 0.18	0.08 ± 0.01	0.59 ± 0.33	0.37 ± 0.23	<b>0.41</b> ± 0.19
HAMSTER(w 3D-DA)	0.46 ± 0.12	<b>0.44</b> ± 0.17	<b>0.29</b> ± 0.14	<b>0.59</b> ± 0.2	<b>0.12</b> ± 0.04	<b>0.65</b> ± 0.2	<b>0.68</b> ± 0.13	0.38 ± 0.11

Table 1: Simulation evaluation of HAMSTER across different visual variations. We test vanilla 3D Diffuser Actor and HAMSTER across variations in Colosseum (Pumacay et al., 2024) and find that HAMSTER generalizes more effectively than 3D Diffuser Actor. Avg. indicates mean across variations, including no variation. For details about each variation, please refer to Pumacay et al. (2024).

## 5.2 SIMULATION EVALUATION

We also perform controlled experiments in simulation. We use Colosseum (Pumacay et al., 2024) as the benchmark as it displays considerable visual and semantic variations. In simulation, we paired our high-level VLM, with 3D Diffuser Actor (Ke et al., 2024) as the low-level policy, since this is one of the state-of-the-art models on RLBench. We compare HAMSTER with a vanilla 3D Diffuser Actor implementation without path guidance. Table. 1 summarizes our results in simulation. HAMSTER significantly outperforms vanilla 3D-DA (0.43 vs 0.52). This shows that the 2D paths produced by the VLM in HAMSTER can help low-level policies to generalize better to novel unseen variations. We refer readers to Colosseum (Pumacay et al., 2024) for details on the variations.

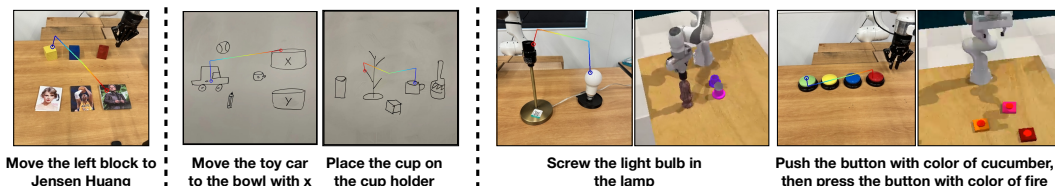
## 5.3 IMPACT OF DESIGN DECISIONS ON VLM PERFORMANCE

To better understand the transfer and generalization performance of the proposed hierarchical VLA model, we analyze the impact of various decisions involved in training the high-level VLM. We conduct a human evaluation of different variants of a trained high-level VLM on a randomly collected dataset of real-world test images, as shown in Figure 5. We ask each model to generate 2D path traces corresponding to instructions such as “move the block on the right to Taylor Swift” or “screw the light bulb in the lamp” (the full set is in Appendix C.1). We then provide the paths generated by each method to human evaluators who have not previously seen any of the models’ predictions. The human evaluators rank the predictions for different methods and the average rank across the samples is reported in Table 2.

We evaluate the following VLM models (listed in the order seen in Table 2): (1) zero-shot state-of-the-art closed-source models such as GPT-4o using a similar prompt to ours (shown in Figure 7) (2) zero-shot state-of-the-art closed-source models such as GPT-4o but using Code-as-Policies (Liang et al., 2023) to generate paths as described in Gu et al. (2023) (3) finetuned open-source models (VILA-1.5-13b) on the data sources described in Section 4.1, but excluding the simulation trajectories from the RLBench dataset, (4) finetuned open-source models (VILA-1.5-13b) on the data

486	Method	VLM	Finetuning Data	Rank Exc. Real RLB.	Rank Real RLB.	Rank All
487	RT-Traj.	0-shot GPT4-o	-	3.40	3.63	3.52
488	RT-Traj.	CaP GPT4-o	-	3.57	3.36	3.46
489	HAMSTER	VILA	Our Exc. Sim RLB.	1.78	2.39	2.11
490	HAMSTER	VILA	Our	<b>1.59</b>	<b>1.28</b>	<b>1.42</b>
491						
492						

493 Table 2: Ranking-based human evaluation of different VLMs, averaged across various real-world evaluation  
 494 tasks. Results indicate that HAMSTER including simulation data is most effective since it captures both spatial  
 495 and semantic information across diverse tasks from RL-Bench. This significantly outperforms zero-shot VLM-  
 496 based trajectory generation, as described in Gu et al. (2023)



505 Figure 5: HAMSTER’s VLM demonstrates considerable generalization and cross-domain learning to scenarios  
 506 not encountered in the training set. From left to right: (a) it can effectively utilize world knowledge to  
 507 generalize to tasks specified by people; (b) it generalizes to highly out-of-domain input images, such as human-  
 508 drawn sketches; (c) when trained on diverse simulated data it shows transfer to related, but visually distinct  
 509 tasks.

510 sources described in Section 4.1, including path sketches from the RL-Bench dataset. The purpose  
 511 of these evaluations is to first compare with closely related work that generates 2D trajectories using  
 512 pretrained closed source VLMs Gu et al. (2023) (Comparison (1) and (2)). The comparison be-  
 513 tween (3) and (4) (our complete method) is meant to isolate the impact of including the simulation  
 514 path sketches from the RL-Bench dataset. In doing so, we analyze the ability of the VLM to pre-  
 515 dict intermediate paths to transfer across significantly varying domains (from RL-Bench to the real  
 516 world).

517 The results suggest that: (1) zero-shot path generation, even from closed-source VLMs Gu et al.  
 518 (2023) such as GPT-4o with additional help through Code-as-Policies (Liang et al., 2023), under-  
 519 performs VLMs finetuned on cross-domain data as in HAMSTER; (2) inclusion of significantly  
 520 different training data such as low-fidelity simulation during finetuning improves the real-world per-  
 521 formance of the VLM. This highlights the transferability displayed by HAMSTER across widely  
 522 varying domains. These results emphasize that the hierarchical VLA approach described in HAM-  
 523 STER can effectively utilize diverse sources of cheap prior data for 2D path predictions, despite  
 524 considerable perceptual differences.

## 525 6 CONCLUSION AND LIMITATIONS

526 In summary, HAMSTER studies the potential of hierarchical VLA models, achieving robust gen-  
 527 eralization in robotic manipulation. It consists of a finetuned VLM that accurately predicts 2D paths  
 528 for robotic manipulation and a low-level policy that learns to generate actions using the 2D paths.  
 529 This two-step architecture enables visual generalization and semantic reasoning across consider-  
 530 able domain shifts, while enabling data-efficient specialist policies, like ones conditioned on 3D inputs,  
 531 to perform low-level action execution.

532 This work represents an initial step towards developing versatile, hierarchical VLA methods, with  
 533 numerous opportunities for future improvement and expansion. The proposed work only generates  
 534 points in 2D space, without making native 3D predictions. This prevents the VLM from having true  
 535 spatial 3D understanding. Moreover, the interface of just using 2D paths is a bandwidth limited one,  
 536 which cannot communicate nuances such as force or rotation. In the future, investigating learnable  
 537 intermediate interfaces is a promising direction. Moreover, training these VLMs directly from large-  
 538 scale human video datasets would also be promising.

540 REFERENCES  
541

542 OpenAI Josh Achiam, Steven Adler, Sandhini Agarwal, Lama Ahmad, Ilge Akkaya, Florencia Leoni  
 543 Aleman, Diogo Almeida, Janko Altenschmidt, Sam Altman, Shyamal Anadkat, Red Avila, Igor  
 544 Babuschkin, Suchir Balaji, Valerie Balcom, Paul Baltescu, Haiming Bao, Mo Bavarian, Jeff Bel-  
 545 gum, Irwan Bello, Jake Berdine, Gabriel Bernadett-Shapiro, Christopher Berner, Lenny Bog-  
 546 donoff, Oleg Boiko, Madelaine Boyd, Anna-Luisa Brakman, Greg Brockman, Tim Brooks, Miles  
 547 Brundage, Kevin Button, Trevor Cai, Rosie Campbell, Andrew Cann, Brittany Carey, Chelsea  
 548 Carlson, Rory Carmichael, Brooke Chan, Che Chang, Fotis Chantzis, Derek Chen, Sully Chen,  
 549 Ruby Chen, Jason Chen, Mark Chen, Benjamin Chess, Chester Cho, Casey Chu, Hyung Won  
 550 Chung, Dave Cummings, Jeremiah Currier, Yunxing Dai, Cory Decareaux, Thomas Degry, Noah  
 551 Deutsch, Damien Deville, Arka Dhar, David Dohan, Steve Dowling, Sheila Dunning, Adrien  
 552 Ecoffet, Atty Eleti, Tyna Eloundou, David Farhi, Liam Fedus, Niko Felix, Sim'on Posada Fish-  
 553 man, Juston Forte, Isabella Fulford, Leo Gao, Elie Georges, Christian Gibson, Vik Goel, Tarun  
 554 Gogineni, Gabriel Goh, Raphael Gontijo-Lopes, Jonathan Gordon, Morgan Grafstein, Scott Gray,  
 555 Ryan Greene, Joshua Gross, Shixiang Shane Gu, Yufei Guo, Chris Hallacy, Jesse Han, Jeff Har-  
 556 rris, Yuchen He, Mike Heaton, Johannes Heidecke, Chris Hesse, Alan Hickey, Wade Hickey, Peter  
 557 Hoeschele, Brandon Houghton, Kenny Hsu, Shengli Hu, Xin Hu, Joost Huizinga, Shantanu Jain,  
 558 Shawn Jain, Joanne Jang, Angela Jiang, Roger Jiang, Haozhun Jin, Denny Jin, Shino Jomoto,  
 559 Billie Jonn, Heewoo Jun, Tomer Kaftan, Lukasz Kaiser, Ali Kamali, Ingmar Kanitscheider, Ni-  
 560 tish Shirish Keskar, Tabarak Khan, Logan Kilpatrick, Jong Wook Kim, Christina Kim, Yongjik  
 561 Kim, Hendrik Kirchner, Jamie Ryan Kiros, Matthew Knight, Daniel Kokotajlo, Lukasz Kon-  
 562 draciuk, Andrew Kondrich, Aris Konstantinidis, Kyle Kosic, Gretchen Krueger, Vishal Kuo,  
 563 Michael Lampe, Ikai Lan, Teddy Lee, Jan Leike, Jade Leung, Daniel Levy, Chak Ming Li,  
 564 Rachel Lim, Molly Lin, Stephanie Lin, Mateusz Litwin, Theresa Lopez, Ryan Lowe, Patricia  
 565 Lue, Anna Adeola Makanju, Kim Malfacini, Sam Manning, Todor Markov, Yaniv Markovski,  
 566 Bianca Martin, Katie Mayer, Andrew Mayne, Bob McGrew, Scott Mayer McKinney, Christine  
 567 McLeavey, Paul McMillan, Jake McNeil, David Medina, Aalok Mehta, Jacob Menick, Luke  
 568 Metz, Andrey Mishchenko, Pamela Mishkin, Vinnie Monaco, Evan Morikawa, Daniel P. Mossing,  
 569 Tong Mu, Mira Murati, Oleg Murk, David M'ely, Ashvin Nair, Reiichiro Nakano, Rajeev Nayak,  
 570 Arvind Neelakantan, Richard Ngo, Hyeonwoo Noh, Ouyang Long, Cullen O'Keefe, Jakub W.  
 571 Pachocki, Alex Paino, Joe Palermo, Ashley Pantuliano, Giambattista Parascandolo, Joel Parish,  
 572 Emy Parparita, Alexandre Passos, Mikhail Pavlov, Andrew Peng, Adam Perelman, Filipe de Avila  
 573 Belbute Peres, Michael Petrov, Henrique Pondé de Oliveira Pinto, Michael Pokorny, Michelle  
 574 Pokrass, Vitchyr H. Pong, Tolly Powell, Alethea Power, Boris Power, Elizabeth Proehl, Raul  
 575 Puri, Alec Radford, Jack Rae, Aditya Ramesh, Cameron Raymond, Francis Real, Kendra Rim-  
 576 bach, Carl Ross, Bob Rotsted, Henri Roussez, Nick Ryder, Mario D. Saltarelli, Ted Sanders,  
 577 Shibani Santurkar, Girish Sastry, Heather Schmidt, David Schnurr, John Schulman, Daniel Sel-  
 578 sam, Kyla Sheppard, Toki Sherbakov, Jessica Shieh, Sarah Shoker, Pranav Shyam, Szymon Sidor,  
 579 Eric Sigler, Maddie Simens, Jordan Sitkin, Katarina Slama, Ian Sohl, Benjamin D. Sokolowsky,  
 580 Yang Song, Natalie Staudacher, Felipe Petroski Such, Natalie Summers, Ilya Sutskever, Jie Tang,  
 581 Nikolas A. Tezak, Madeleine Thompson, Phil Tillet, Amin Tootoonchian, Elizabeth Tseng, Pre-  
 582 ston Tuggle, Nick Turley, Jerry Tworek, Juan Felipe Cer'on Uribe, Andrea Vallone, Arun Vi-  
 583 jayvergyia, Chelsea Voss, Carroll L. Wainwright, Justin Jay Wang, Alvin Wang, Ben Wang,  
 584 Jonathan Ward, Jason Wei, CJ Weinmann, Akila Welihinda, Peter Welinder, Jiayi Weng, Lilian  
 585 Weng, Matt Wiethoff, Dave Willner, Clemens Winter, Samuel Wolrich, Hannah Wong, Lauren  
 Workman, Sherwin Wu, Jeff Wu, Michael Wu, Kai Xiao, Tao Xu, Sarah Yoo, Kevin Yu, Qiming  
 Yuan, Wojciech Zaremba, Rowan Zellers, Chong Zhang, Marvin Zhang, Shengjia Zhao, Tian-  
 hao Zheng, Juntang Zhuang, William Zhuk, and Barret Zoph. Gpt-4 technical report. In *arxiv*  
 preprint, 2023. URL <https://arxiv.org/pdf/2303.08774.pdf>.

586 Jinze Bai, Shuai Bai, Shusheng Yang, Shijie Wang, Sinan Tan, Peng Wang, Junyang Lin, Chang  
 587 Zhou, and Jingren Zhou. Qwen-vl: A frontier large vision-language model with versatile abilities.  
 588 *arXiv preprint arXiv:2308.12966*, 2023.

589 Anthony Brohan, Noah Brown, Justice Carbajal, Yevgen Chebotar, Joseph Dabis, Chelsea Finn,  
 590 Keerthana Gopalakrishnan, Karol Hausman, Alex Herzog, Jasmine Hsu, et al. Rt-1: Robotics  
 591 transformer for real-world control at scale. *arXiv preprint arXiv:2212.06817*, 2022.

592 Anthony Brohan, Noah Brown, Justice Carbajal, Yevgen Chebotar, Xi Chen, Krzysztof Choro-  
 593 manski, Tianli Ding, Danny Driess, Avinava Dubey, Chelsea Finn, Pete Florence, Chuyuan Fu,

- 594 Montse Gonzalez Arenas, Keerthana Gopalakrishnan, Kehang Han, Karol Hausman, Alex Herzog,  
 595 Jasmine Hsu, Brian Ichter, Alex Irpan, Nikhil Joshi, Ryan Julian, Dmitry Kalashnikov,  
 596 Yuheng Kuang, Isabel Leal, Lisa Lee, Tsang-Wei Edward Lee, Sergey Levine, Yao Lu, Hen-  
 597 ryk Michalewski, Igor Mordatch, Karl Pertsch, Kanishka Rao, Krista Reymann, Michael Ryoo,  
 598 Grecia Salazar, Pannag Sanketi, Pierre Sermanet, Jaspia Singh, Anikait Singh, Radu Soricu-  
 599 tran, Huong Tran, Vincent Vanhoucke, Quan Vuong, Ayzaan Wahid, Stefan Welker, Paul Wohlhart,  
 600 Jialin Wu, Fei Xia, Ted Xiao, Peng Xu, Sichun Xu, Tianhe Yu, and Brianna Zitkovich. Rt-  
 601 2: Vision-language-action models transfer web knowledge to robotic control. In *arXiv preprint  
 arXiv:2307.15818*, 2023a.
- 603 Anthony Brohan, Yevgen Chebotar, Chelsea Finn, Karol Hausman, Alexander Herzog, Daniel Ho,  
 604 Julian Ibarz, Alex Irpan, Eric Jang, Ryan Julian, et al. Do as i can, not as i say: Grounding  
 605 language in robotic affordances. In *Conference on robot learning*, pp. 287–318. PMLR, 2023b.  
 606
- 607 Minwoo Byeon, Beomhee Park, Haecheon Kim, Sungjun Lee, Woonhyuk Baek, and Saehoon  
 608 Kim. Coyo-700m: Image-text pair dataset. [https://github.com/kakaobrain/  
 609 coyo-dataset](https://github.com/kakaobrain/coyo-dataset), 2022.
- 610 Cheng Chi, Siyuan Feng, Yilun Du, Zhenjia Xu, Eric Cousineau, Benjamin Burchfiel, and Shuran  
 611 Song. Diffusion policy: Visuomotor policy learning via action diffusion. In Kostas E. Bekris,  
 612 Kris Hauser, Sylvia L. Herbert, and Jingjin Yu (eds.), *Robotics: Science and Systems XIX, Daegu,  
 613 Republic of Korea, July 10-14, 2023*, 2023. doi: 10.15607/RSS.2023.XIX.026. URL <https://doi.org/10.15607/RSS.2023.XIX.026>.
- 615 Open X-Embodiment Collaboration, Abby O'Neill, Abdul Rehman, Abhinav Gupta, Abhiram Mad-  
 616 dukuri, Abhishek Gupta, Abhishek Padalkar, Abraham Lee, Acorn Pooley, Agrim Gupta, Ajay  
 617 Mandlekar, Ajinkya Jain, Albert Tung, Alex Bewley, Alex Herzog, Alex Irpan, Alexander Khaz-  
 618 atsky, Anant Rai, Anchit Gupta, Andrew Wang, Andrey Kolobov, Anikait Singh, Animesh Garg,  
 619 Aniruddha Kembhavi, Annie Xie, Anthony Brohan, Antonin Raffin, Archit Sharma, Arefeh  
 620 Yavary, Arhan Jain, Ashwin Balakrishna, Ayzaan Wahid, Ben Burgess-Limerick, Beomjoon Kim,  
 621 Bernhard Schölkopf, Blake Wulfe, Brian Ichter, Cewu Lu, Charles Xu, Charlotte Le, Chelsea  
 622 Finn, Chen Wang, Chenfeng Xu, Cheng Chi, Chenguang Huang, Christine Chan, Christopher  
 623 Agia, Chuer Pan, Chuyuan Fu, Coline Devin, Danfei Xu, Daniel Morton, Danny Driess, Daphne  
 624 Chen, Deepak Pathak, Dhruv Shah, Dieter Büchler, Dinesh Jayaraman, Dmitry Kalashnikov,  
 625 Dorsa Sadigh, Edward Johns, Ethan Foster, Fangchen Liu, Federico Ceola, Fei Xia, Feiyu Zhao,  
 626 Felipe Vieira Frujeri, Freek Stulp, Gaoyue Zhou, Gaurav S. Sukhatme, Gautam Salhotra, Ge Yan,  
 627 Gilbert Feng, Giulio Schiavi, Glen Berseth, Gregory Kahn, Guangwen Yang, Guanzhi Wang, Hao  
 628 Su, Hao-Shu Fang, Haochen Shi, Henghui Bao, Heni Ben Amor, Henrik I Christensen, Hiroki  
 629 Furuta, Homanga Bharadhwaj, Homer Walke, Hongjie Fang, Huy Ha, Igor Mordatch, Ilija Ra-  
 630 dosavovic, Isabel Leal, Jacky Liang, Jad Abou-Chakra, Jaehyung Kim, Jaimyn Drake, Jan Peters,  
 631 Jan Schneider, Jasmine Hsu, Jay Vakil, Jeannette Bohg, Jeffrey Bingham, Jeffrey Wu, Jensen  
 632 Gao, Jiaheng Hu, Jiajun Wu, Jialin Wu, Jiankai Sun, Jianlan Luo, Jiayuan Gu, Jie Tan, Jihoon  
 633 Oh, Jimmy Wu, Jingpei Lu, Jingyun Yang, Jitendra Malik, João Silvério, Joey Hejna, Jonathan  
 634 Booher, Jonathan Tompson, Jonathan Yang, Jordi Salvador, Joseph J. Lim, Junhyek Han, Kaiyuan  
 635 Wang, Kanishka Rao, Karl Pertsch, Karol Hausman, Keegan Go, Keerthana Gopalakrishnan, Ken  
 636 Goldberg, Kendra Byrne, Kenneth Oslund, Kento Kawaharazuka, Kevin Black, Kevin Lin, Kevin  
 637 Zhang, Kiana Ehsani, Kiran Lekkala, Kirsty Ellis, Krishnan Rana, Krishnan Srinivasan, Kuan  
 638 Fang, Kunal Pratap Singh, Kuo-Hao Zeng, Kyle Hatch, Kyle Hsu, Laurent Itti, Lawrence Yun-  
 639 liang Chen, Lerrel Pinto, Li Fei-Fei, Liam Tan, Linxi "Jim" Fan, Lionel Ott, Lisa Lee, Luca  
 640 Weihs, Magnum Chen, Marion Lepert, Marius Memmel, Masayoshi Tomizuka, Masha Itkina,  
 641 Mateo Guaman Castro, Max Spero, Maximilian Du, Michael Ahn, Michael C. Yip, Mingtong  
 642 Zhang, Mingyu Ding, Minho Heo, Mohan Kumar Srirama, Mohit Sharma, Moo Jin Kim, Naoaki  
 643 Kanazawa, Nicklas Hansen, Nicolas Heess, Nikhil J Joshi, Niko Suenderhauf, Ning Liu, Nor-  
 644 man Di Palo, Nur Muhammad Mahi Shafullah, Oier Mees, Oliver Kroemer, Osbert Bastani,  
 645 Pannag R Sanketi, Patrick "Tree" Miller, Patrick Yin, Paul Wohlhart, Peng Xu, Peter David  
 646 Fagan, Peter Mitrano, Pierre Sermanet, Pieter Abbeel, Priya Sundaresan, Qiuyu Chen, Quan  
 647 Vuong, Rafael Rafailov, Ran Tian, Ria Doshi, Roberto Mart'in-Mart'in, Rohan Baijal, Rosario  
 Scalise, Rose Hendrix, Roy Lin, Runjia Qian, Ruohan Zhang, Russell Mendonca, Rutav Shah,  
 Ryan Hoque, Ryan Julian, Samuel Bustamante, Sean Kirmani, Sergey Levine, Shan Lin, Sherry  
 Moore, Shikhar Bahl, Shivin Dass, Shubham Sonawani, Shubham Tulsiani, Shuran Song, Sichun

- 648 Xu, Siddhant Haldar, Siddharth Karamcheti, Simeon Adebola, Simon Guist, Soroush Nasiriany,  
 649 Stefan Schaal, Stefan Welker, Stephen Tian, Subramanian Ramamoorthy, Sudeep Dasari, Suneel  
 650 Belkhale, Sungjae Park, Suraj Nair, Suvir Mirchandani, Takayuki Osa, Tanmay Gupta, Tatsuya  
 651 Harada, Tatsuya Matsushima, Ted Xiao, Thomas Kollar, Tianhe Yu, Tianli Ding, Todor Davchev,  
 652 Tony Z. Zhao, Travis Armstrong, Trevor Darrell, Trinity Chung, Vidhi Jain, Vikash Kumar, Vin-  
 653 cent Vanhoucke, Wei Zhan, Wenxuan Zhou, Wolfram Burgard, Xi Chen, Xiangyu Chen, Xiaolong  
 654 Wang, Xinghao Zhu, Xinyang Geng, Xiyuan Liu, Xu Liangwei, Xuanlin Li, Yansong Pang, Yao  
 655 Lu, Yecheng Jason Ma, Yejin Kim, Yevgen Chebotar, Yifan Zhou, Yifeng Zhu, Yilin Wu, Ying  
 656 Xu, Yixuan Wang, Yonatan Bisk, Yongqiang Dou, Yoonyoung Cho, Youngwoon Lee, Yuchen  
 657 Cui, Yue Cao, Yueh-Hua Wu, Yujin Tang, Yuke Zhu, Yunchu Zhang, Yunfan Jiang, Yunshuang  
 658 Li, Yunzhu Li, Yusuke Iwasawa, Yutaka Matsuo, Zehan Ma, Zhuo Xu, Zichen Jeff Cui, Zichen  
 659 Zhang, Zipeng Fu, and Zipeng Lin. Open X-Embodiment: Robotic learning datasets and RT-X  
 660 models. <https://arxiv.org/abs/2310.08864>, 2023.
- 661 Carl Doersch, Yi Yang, Mel Vecerik, Dilara Gokay, Ankush Gupta, Yusuf Aytar, Joao Carreira,  
 662 and Andrew Zisserman. Tapir: Tracking any point with per-frame initialization and temporal  
 663 refinement. In *Proceedings of the IEEE/CVF International Conference on Computer Vision*, pp.  
 664 10061–10072, 2023.
- 665 David H Douglas and Thomas K Peucker. Algorithms for the reduction of the number of  
 666 points required to represent a digitized line or its caricature. *Cartographica*, 10(2):112–  
 667 122, 1973. doi: 10.3138/FM57-6770-U75U-7727. URL [https://doi.org/10.3138/  
 668 FM57-6770-U75U-7727](https://doi.org/10.3138/FM57-6770-U75U-7727).
- 669 Danny Driess, Fei Xia, Mehdi SM Sajjadi, Corey Lynch, Aakanksha Chowdhery, Brian Ichter,  
 670 Ayzaan Wahid, Jonathan Tompson, Quan Vuong, Tianhe Yu, et al. Palm-e: An embodied mul-  
 671 timodal language model. In *International Conference on Machine Learning*, pp. 8469–8488.  
 672 PMLR, 2023.
- 673 Adam Fishman, Adithyavairavan Murali, Clemens Eppner, Bryan Peele, Byron Boots, and Dieter  
 674 Fox. Motion policy networks. In Karen Liu, Dana Kulic, and Jeffrey Ichnowski (eds.), *Conference  
 675 on Robot Learning, CoRL 2022, 14–18 December 2022, Auckland, New Zealand*, volume 205  
 676 of *Proceedings of Machine Learning Research*, pp. 967–977. PMLR, 2022. URL <https://proceedings.mlr.press/v205/fishman23a.html>.
- 677 Ankit Goyal, Jie Xu, Yijie Guo, Valts Blukis, Yu-Wei Chao, and Dieter Fox. Rvt: Robotic view  
 678 transformer for 3d object manipulation. In *Conference on Robot Learning*, pp. 694–710. PMLR,  
 679 2023.
- 680 Ankit Goyal, Valts Blukis, Jie Xu, Yijie Guo, Yu-Wei Chao, and Dieter Fox. Rvt2: Learning precise  
 681 manipulation from few demonstrations. *RSS*, 2024.
- 682 Jiayuan Gu, Sean Kirmani, Paul Wohlhart, Yao Lu, Montserrat Gonzalez Arenas, Kanishka Rao,  
 683 Wenhao Yu, Chuyuan Fu, Keerthana Gopalakrishnan, Zhuo Xu, Priya Sundaresan, Peng Xu,  
 684 Hao Su, Karol Hausman, Chelsea Finn, Quan Vuong, and Ted Xiao. Rt-trajectory: Robotic task  
 685 generalization via hindsight trajectory sketches, 2023.
- 686 Ankur Handa, Arthur Allshire, Viktor Makoviychuk, Aleksei Petrenko, Ritvik Singh, Jingzhou Liu,  
 687 Denys Makoviichuk, Karl Van Wyk, Alexander Zhurkevich, Balakumar Sundaralingam, et al.  
 688 Dextreme: Transfer of agile in-hand manipulation from simulation to reality. In *2023 IEEE  
 689 International Conference on Robotics and Automation (ICRA)*, pp. 5977–5984. IEEE, 2023.
- 690 Wenlong Huang, Pieter Abbeel, Deepak Pathak, and Igor Mordatch. Language models as zero-shot  
 691 planners: Extracting actionable knowledge for embodied agents. In *International conference on  
 692 machine learning*, pp. 9118–9147. PMLR, 2022.
- 693 Wenlong Huang, Chen Wang, Ruohan Zhang, Yunzhu Li, Jiajun Wu, and Li Fei-Fei. Voxposer:  
 694 Composable 3d value maps for robotic manipulation with language models. In *Conference on  
 695 Robot Learning*, pp. 540–562. PMLR, 2023a.
- 696 Wenlong Huang, Fei Xia, Ted Xiao, Harris Chan, Jacky Liang, Pete Florence, Andy Zeng, Jonathan  
 697 Tompson, Igor Mordatch, Yevgen Chebotar, et al. Inner monologue: Embodied reasoning through  
 698 701

- 702 planning with language models. In *Conference on Robot Learning*, pp. 1769–1782. PMLR,  
 703 2023b.
- 704
- 705 Stephen James, Zicong Ma, David Rovick Arrojo, and Andrew J Davison. Rlbench: The robot  
 706 learning benchmark & learning environment. *IEEE Robotics and Automation Letters*, 5(2):3019–  
 707 3026, 2020.
- 708 Eric Jang, Alex Irpan, Mohi Khansari, Daniel Kappler, Frederik Ebert, Corey Lynch, Sergey Levine,  
 709 and Chelsea Finn. Bc-z: Zero-shot task generalization with robotic imitation learning. In *Confer-  
 710 ence on Robot Learning*, pp. 991–1002. PMLR, 2022.
- 711
- 712 Yunfan Jiang, Agrim Gupta, Zichen Zhang, Guanzhi Wang, Yongqiang Dou, Yanjun Chen, Li Fei-  
 713 Fei, Anima Anandkumar, Yuke Zhu, and Linxi Fan. Vima: General robot manipulation with  
 714 multimodal prompts. In *International Conference on Machine Learning*, 2023.
- 715 Tsung-Wei Ke, Nikolaos Gkanatsios, and Katerina Fragkiadaki. 3d diffuser actor: Policy diffusion  
 716 with 3d scene representations. In *First Workshop on Vision-Language Models for Navigation and  
 717 Manipulation at ICRA 2024*, 2024.
- 718
- 719 Alexander Khazatsky, Karl Pertsch, Suraj Nair, Ashwin Balakrishna, Sudeep Dasari, Siddharth  
 720 Karamcheti, Soroush Nasiriany, Mohan Kumar Srirama, Lawrence Yunliang Chen, Kirsty Ellis,  
 721 Peter David Fagan, Joey Hejna, Masha Itkina, Marion Lepert, Yecheng Jason Ma, Patrick Tree  
 722 Miller, Jimmy Wu, Suneel Belkhale, Shivin Dass, Huy Ha, Arhan Jain, Abraham Lee, Young-  
 723 woon Lee, Marius Memmel, Sungjae Park, Ilija Radosavovic, Kaiyuan Wang, Albert Zhan, Kevin  
 724 Black, Cheng Chi, Kyle Beltran Hatch, Shan Lin, Jingpei Lu, Jean Mercat, Abdul Rehman, Pan-  
 725 ntag R Sanketi, Archit Sharma, Cody Simpson, Quan Vuong, Homer Rich Walke, Blake Wulfe,  
 726 Ted Xiao, Jonathan Heewon Yang, Arefeh Yavary, Tony Z. Zhao, Christopher Agia, Rohan Bai-  
 727 jal, Mateo Guaman Castro, Daphne Chen, Qiyu Chen, Trinity Chung, Jaimyn Drake, Ethan Paul  
 728 Foster, Jensen Gao, David Antonio Herrera, Minho Heo, Kyle Hsu, Jiaheng Hu, Donovan Jack-  
 729 son, Charlotte Le, Yunshuang Li, Kevin Lin, Roy Lin, Zehan Ma, Abhiram Maddukuri, Suvir Mir-  
 730 chandani, Daniel Morton, Tony Nguyen, Abigail O'Neill, Rosario Scalise, Derick Seale, Victor  
 731 Son, Stephen Tian, Emi Tran, Andrew E. Wang, Yilin Wu, Annie Xie, Jingyun Yang, Patrick Yin,  
 732 Yunchu Zhang, Osbert Bastani, Glen Berseth, Jeannette Bohg, Ken Goldberg, Abhinav Gupta,  
 733 Abhishek Gupta, Dinesh Jayaraman, Joseph J Lim, Jitendra Malik, Roberto Martín-Martín, Sub-  
 734 ramanian Ramamoorthy, Dorsa Sadigh, Shuran Song, Jiajun Wu, Michael C. Yip, Yuke Zhu,  
 735 Thomas Kollar, Sergey Levine, and Chelsea Finn. Droid: A large-scale in-the-wild robot manip-  
 736 ulation dataset. 2024.
- 737
- 738 Moo Jin Kim, Karl Pertsch, Siddharth Karamcheti, Ted Xiao, Ashwin Balakrishna, Suraj Nair,  
 739 Rafael Rafailov, Ethan Foster, Grace Lam, Pannag Sanketi, et al. Openvla: An open-source  
 740 vision-language-action model. *arXiv preprint arXiv:2406.09246*, 2024.
- 741
- 742 Minae Kwon, Sang Michael Xie, Kalesha Bullard, and Dorsa Sadigh. Reward design with language  
 743 models. In *The Eleventh International Conference on Learning Representations*, 2023.
- 744
- 745 Joonho Lee, Jemin Hwangbo, Lorenz Wellhausen, Vladlen Koltun, and Marco Hutter. Learning  
 746 quadrupedal locomotion over challenging terrain. *Science robotics*, 5(47):eabc5986, 2020.
- 747
- 748 Jacky Liang, Wenlong Huang, Fei Xia, Peng Xu, Karol Hausman, Brian Ichter, Pete Florence, and  
 749 Andy Zeng. Code as policies: Language model programs for embodied control. In *2023 IEEE  
 750 International Conference on Robotics and Automation (ICRA)*, pp. 9493–9500. IEEE, 2023.
- 751
- 752 Ji Lin, Hongxu Yin, Wei Ping, Pavlo Molchanov, Mohammad Shoeybi, and Song Han. Vila: On pre-  
 753 training for visual language models. In *Proceedings of the IEEE/CVF Conference on Computer  
 754 Vision and Pattern Recognition (CVPR)*, pp. 26689–26699, June 2024.
- 755
- 756 Fangchen Liu, Kuan Fang, Pieter Abbeel, and Sergey Levine. Moka: Open-vocabulary robotic  
 757 manipulation through mark-based visual prompting. *arXiv preprint arXiv:2403.03174*, 2024a.

- 756 Haotian Liu, Chunyuan Li, Qingyang Wu, and Yong Jae Lee. Visual instruction tuning. *Advances*  
 757 *in neural information processing systems*, 36, 2024b.  
 758
- 759 Pan Lu, Swaroop Mishra, Tony Xia, Liang Qiu, Kai-Wei Chang, Song-Chun Zhu, Oyvind Tafjord,  
 760 Peter Clark, and Ashwin Kalyan. Learn to explain: Multimodal reasoning via thought chains for  
 761 science question answering. In *The 36th Conference on Neural Information Processing Systems*  
 762 (*NeurIPS*), 2022.
- 763 Yecheng Jason Ma, Shagun Sodhani, Dinesh Jayaraman, Osbert Bastani, Vikash Kumar, and Amy  
 764 Zhang. Vip: Towards universal visual reward and representation via value-implicit pre-training.  
 765 In *The Eleventh International Conference on Learning Representations*, 2023.
- 766 Yecheng Jason Ma, William Liang, Guanzhi Wang, De-An Huang, Osbert Bastani, Dinesh Jayara-  
 767 man, Yuke Zhu, Linxi Fan, and Anima Anandkumar. Eureka: Human-level reward design via  
 768 coding large language models. In *The Twelfth International Conference on Learning Representa-  
 769 tions*, 2024.
- 770 Ajay Mandlekar, Soroush Nasiriany, Bowen Wen, Iretiayo Akinola, Yashraj Narang, Linxi Fan,  
 771 Yuke Zhu, and Dieter Fox. Mimicgen: A data generation system for scalable robot learning using  
 772 human demonstrations. In *Conference on Robot Learning*, pp. 1820–1864. PMLR, 2023.
- 773 Matthias Minderer, Alexey Gritsenko, Austin Stone, Maxim Neumann, Dirk Weissenborn, Alexey  
 774 Dosovitskiy, Aravindh Mahendran, Anurag Arnab, Mostafa Dehghani, Zhuoran Shen, et al. Sim-  
 775 ple open-vocabulary object detection. In *European Conference on Computer Vision*, pp. 728–755.  
 776 Springer, 2022.
- 777 Suraj Nair, Aravind Rajeswaran, Vikash Kumar, Chelsea Finn, and Abhinav Gupta. R3m: A univer-  
 778 sal visual representation for robot manipulation. In *Conference on Robot Learning*, pp. 892–909.  
 779 PMLR, 2023.
- 780 Soroush Nasiriany, Fei Xia, Wenhao Yu, Ted Xiao, Jacky Liang, Ishita Dasgupta, Annie Xie, Danny  
 781 Driess, Ayzaan Wahid, Zhuo Xu, et al. Pivot: Iterative visual prompting elicits actionable knowl-  
 782 edge for vlms. In *International Conference on Machine Learning*, 2024.
- 783 Dantong Niu, Yuvan Sharma, Giscard Biamby, Jerome Quenum, Yutong Bai, Baifeng Shi, Trevor  
 784 Darrell, and Roei Herzig. LLARVA: Vision-action instruction tuning enhances robot learning.  
 785 In *8th Annual Conference on Robot Learning*, 2024. URL [https://openreview.net/  
 786 forum?id=Q21GXMZCv8](https://openreview.net/forum?id=Q21GXMZCv8).
- 787 Simone Parisi, Aravind Rajeswaran, Senthil Purushwalkam, and Abhinav Gupta. The unsurprising  
 788 effectiveness of pre-trained vision models for control. In *international conference on machine  
 789 learning*, pp. 17359–17371. PMLR, 2022.
- 790 Wilbert Pumacay, Ishika Singh, Jiafei Duan, Ranjay Krishna, Jesse Thomason, and Dieter Fox. The  
 791 colosseum: A benchmark for evaluating generalization for robotic manipulation. *arXiv preprint  
 792 arXiv:2402.08191*, 2024.
- 793 Ilija Radosavovic, Baifeng Shi, Letian Fu, Ken Goldberg, Trevor Darrell, and Jitendra Malik. Robot  
 794 learning with sensorimotor pre-training. In *Conference on Robot Learning*, pp. 683–693. PMLR,  
 795 2023.
- 796 Urs Ramer. An iterative procedure for the polygonal approximation of plane curves. *Computer  
 797 Graphics and Image Processing*, 1(3):244–256, 1972. ISSN 0146-664X. doi: [https://doi.org/10.  
 798 1016/S0146-664X\(72\)80017-0](https://doi.org/10.1016/S0146-664X(72)80017-0). URL [https://www.sciencedirect.com/science/  
 799 article/pii/S0146664X72800170](https://www.sciencedirect.com/science/article/pii/S0146664X72800170).
- 800 Rutav M Shah and Vikash Kumar. Rrl: Resnet as representation for reinforcement learning. In  
 801 *International Conference on Machine Learning*, pp. 9465–9476. PMLR, 2021.
- 802 Zejiang Shen, Kyle Lo, Lucy Lu Wang, Bailey Kuehl, Daniel S. Weld, and Doug Downey. Incor-  
 803 porating visual layout structures for scientific text classification. *ArXiv*, abs/2106.00676, 2021.  
 804 URL <https://arxiv.org/abs/2106.00676>.

- 810 Mohit Shridhar, Lucas Manuelli, and Dieter Fox. Perceiver-actor: A multi-task transformer for  
 811 robotic manipulation. In *Conference on Robot Learning*, pp. 785–799. PMLR, 2023.
- 812 Ishika Singh, Valts Blukis, Arsalan Mousavian, Ankit Goyal, Danfei Xu, Jonathan Tremblay, Dieter  
 813 Fox, Jesse Thomason, and Animesh Garg. Progprompt: Generating situated robot task plans using  
 814 large language models. In *2023 IEEE International Conference on Robotics and Automation*  
 815 (*ICRA*), pp. 11523–11530. IEEE, 2023.
- 816 Sumedh Anand Sontakke, Jesse Zhang, Séb Arnold, Karl Pertsch, Erdem Biyik, Dorsa Sadigh,  
 817 Chelsea Finn, and Laurent Itti. Roboclip: One demonstration is enough to learn robot policies. In  
 818 *NeurIPS*, 2023.
- 819 Austin Stone, Ted Xiao, Yao Lu, Keerthana Gopalakrishnan, Kuang-Huei Lee, Quan Vuong, Paul  
 820 Wohlhart, Sean Kirmani, Brianna Zitkovich, Fei Xia, et al. Open-world object manipulation using  
 821 pre-trained vision-language models. In *Conference on Robot Learning*, pp. 3397–3417. PMLR,  
 822 2023.
- 823 Priya Sundaresan, Suneel Belkhale, Dorsa Sadigh, and Jeannette Bohg. Kite: Keypoint-conditioned  
 824 policies for semantic manipulation. In *Conference on Robot Learning*, pp. 1006–1021. PMLR,  
 825 2023.
- 826 Octo Model Team, Dibya Ghosh, Homer Walke, Karl Pertsch, Kevin Black, Oier Mees, Sudeep  
 827 Dasari, Joey Hejna, Tobias Kreiman, Charles Xu, et al. Octo: An open-source generalist robot  
 828 policy. *arXiv preprint arXiv:2405.12213*, 2024.
- 829 Marcel Torne, Anthony Simeonov, Zechu Li, April Chan, Tao Chen, Abhishek Gupta, and Pulkit  
 830 Agrawal. Reconciling reality through simulation: A real-to-sim-to-real approach for robust ma-  
 831 nipulation. *Robotics: Science and Systems*, 2024.
- 832 Ashish Vaswani, Noam Shazeer, Niki Parmar, Jakob Uszkoreit, Llion Jones, Aidan N. Gomez,  
 833 Lukasz Kaiser, and Illia Polosukhin. Attention is all you need, 2023. URL <https://arxiv.org/abs/1706.03762>.
- 834 Homer Walke, Kevin Black, Abraham Lee, Moo Jin Kim, Max Du, Chongyi Zheng, Tony Zhao,  
 835 Philippe Hansen-Estruch, Quan Vuong, Andre He, Vivek Myers, Kuan Fang, Chelsea Finn, and  
 836 Sergey Levine. Bridgedata v2: A dataset for robot learning at scale. In *Conference on Robot  
 837 Learning (CoRL)*, 2023.
- 838 Yufei Wang, Zhanyi Sun, Jesse Zhang, Zhou Xian, Erdem Biyik, David Held, and Zackory Erick-  
 839 son. Rl-vlm-f: Reinforcement learning from vision language foundation model feedback. In  
 840 *International Conference on Machine Learning*, 2024.
- 841 Wenhao Yu, Nimrod Gileadi, Chuyuan Fu, Sean Kirmani, Kuang-Huei Lee, Montserrat Gonzalez  
 842 Arenas, Hao-Tien Lewis Chiang, Tom Erez, Leonard Hasenclever, Jan Humplík, et al. Language  
 843 to rewards for robotic skill synthesis. In *Conference on Robot Learning*, pp. 374–404. PMLR,  
 844 2023.
- 845 Wentao Yuan, Jiafei Duan, Valts Blukis, Wilbert Pumacay, Ranjay Krishna, Adithyavairavan Murali,  
 846 Arsalan Mousavian, and Dieter Fox. Robopoint: A vision-language model for spatial affordance  
 847 prediction in robotics. In *8th Annual Conference on Robot Learning*, 2024. URL <https://openreview.net/forum?id=GVX6jpZOHU>.
- 848 Tony Z. Zhao, Vikash Kumar, Sergey Levine, and Chelsea Finn. Learning fine-grained bimanual  
 849 manipulation with low-cost hardware. In Kostas E. Bekris, Kris Hauser, Sylvia L. Herbert, and  
 850 Jingjin Yu (eds.), *Robotics: Science and Systems XIX, Daegu, Republic of Korea, July 10-14,*  
 851 2023, 2023. doi: 10.15607/RSS.2023.XIX.016. URL <https://doi.org/10.15607/RSS.2023.XIX.016>.
- 852 Wanrong Zhu, Jack Hessel, Anas Awadalla, Samir Yitzhak Gadre, Jesse Dodge, Alex Fang, Young-  
 853 jae Yu, Ludwig Schmidt, William Yang Wang, and Yejin Choi. Multimodal C4: An open, billion-  
 854 scale corpus of images interleaved with text. *arXiv preprint arXiv:2304.06939*, 2023.
- 855 Brianna Zitkovich, Tianhe Yu, Sichun Xu, Peng Xu, Ted Xiao, Fei Xia, Jialin Wu, Paul Wohlhart,  
 856 Stefan Welker, Ayzaan Wahid, et al. Rt-2: Vision-language-action models transfer web knowledge  
 857 to robotic control. In *Conference on Robot Learning*, pp. 2165–2183. PMLR, 2023.

864 For extended supplementary details and results, please see [https://sites.google.com/  
view/hamster-iclr](https://sites.google.com/view/hamster-iclr).  
865  
866

## 867 A VLM FINETUNING DATASET DETAILS 868

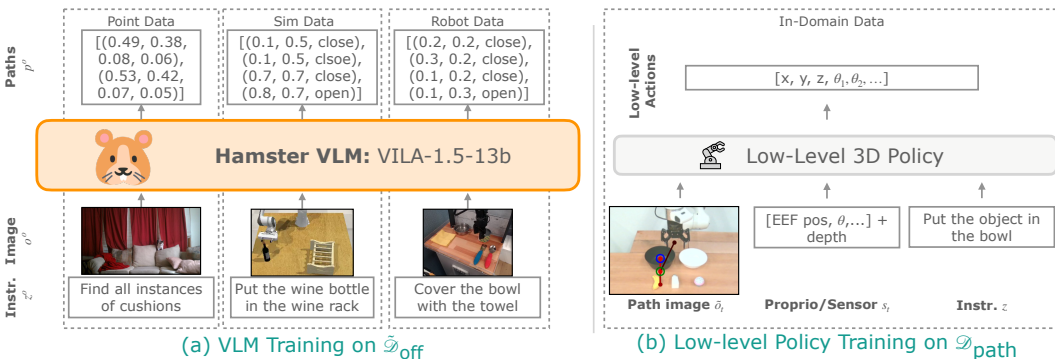
869  
870 **Pixel Point Pred Data.** Our point prediction dataset comes from Robopoint (Yuan et al., 2024).  
871 Most data in our point prediction dataset contains labels given as a set of unordered points such as  
872  $p^o = [(0.25, 0.11), (0.22, 0.19), (0.53, 0.23)]$ . However, data in RoboPoint also contains answers  
873 that are instead in natural language for VQA queries such as “what is the person feeding the cat?” We  
874 keep these data as is because these VQA queries are likely to benefit a VLM’s semantic reasoning and  
875 visual generalization capabilities; we fine-tune HAMSTER’s VLM on the entire Robopoint dataset  
876 as given.  
877

878 **Simulation Data.** We selected 79 RLbench tasks out of 100 to generate data by removing the  
879 tasks with poor visibility on the `front_cam` view in RLbench. We use the first image in each  
880 episodes combined with each language instruction. The final dataset is around 320k.  
881

882 **Real Robot Data.** For the Bridge Walke et al. (2023) dataset, which only provides RGB images,  
883 we extract trajectories by iteratively estimating the extrinsic matrix for each episode. In each scene,  
884 we randomly sample a few frames and manually label the center of the gripper fingers. Using the  
885 corresponding end-effector poses, we compute the 3D-2D projection matrix with a PnP (Perspective-  
886 n-Point) approach. We then apply this projection matrix to the episodes and manually check for any  
887 misalignments between the projected gripper and the actual gripper. Episodes exhibiting significant  
888 deviations are filtered out and start a new round to estimate their extrinsic.  
889

890 For DROID (Khazatsky et al., 2024), a large portion of the dataset contains noisy camera extrinsics  
891 information that do not result in good depth alignment. Therefore, we filter out trajectories with  
892 poor-quality extrinsics as measured by the alignment between the projected depth images and the  
893 RGB images. This results in  $\sim 45k$  trajectories ( $\sim 22k$  unique trajectories as trajectories each have  
894 2 different camera viewpoints) which we use for constructing the VLM dataset  $\mathcal{D}_{\text{off}}$  as described in  
895 Section 4.1.  
896

## 897 B IMPLEMENTATION AND ARCHITECTURE DETAILS 898



900 Figure 6: (a): Examples of training data in  $\tilde{\mathcal{D}}_{\text{off}}$  used to train HAMSTER’s VLM. (b): The data used  
901 to train HAMSTER’s low-level policies.  
902  
903

### 904 B.1 VLM IMPLEMENTATION DETAILS 905

906 **VLM Prompt.** We list the prompt for both fine-tuning on sim and real robot data and evaluation in  
907 Figure 7. We condition the model on an image and the prompt, except when training on Pixel Point  
908 Prediction data (i.e., Robopoint (Yuan et al., 2024) data) where we used the given prompts from the  
909 dataset.  
910

918  
919  
920  
921  
922  
923  
924  
925  
926**HAMSTER Prompt**

In the image, please execute the command described in `<quest>{quest}</quest>`. Provide a sequence of points denoting the trajectory of a robot gripper to achieve the goal. Format your answer as a list of tuples enclosed by `<ans>` and `</ans>` tags. For example: `<ans>[(0.25, 0.32), (0.32, 0.17), (0.13, 0.24), <action>Open Gripper</action>, (0.74, 0.21), <action>Close Gripper</action>, ...]</ans>` The tuple denotes point x and y location of the end effector of the gripper in the image. The action tags indicate the gripper action. The coordinates should be floats ranging between 0 and 1, indicating the relative locations of the points in the image.

927  
928  
929

Figure 7: The full text prompt we use to train HAMSTER with on simulation and real robot data (Section 4.1). We also use this prompt for inference.

930  
931  
932  
933  
934  
935  
936

**VLM Trajectory Shortening.** As mentioned in Section 4.1, one problem with directly training on the path labels  $p^o$  is that many paths may be extremely long. Therefore, we simplify the paths  $p^o$  with the Ramer-Douglas-Peucker algorithm (Ramer, 1972; Douglas & Peucker, 1973) that reduces curves composed of line segments to similar curves composed of fewer points. We run this algorithm on paths produced by simulation and real robot data to generate the labels  $p^o$  for  $\mathcal{D}_{\text{off}}$ . We use tolerance  $\epsilon = 0.05$ .

937  
938  
939  
940  
941

**VLM Training Details.** We train our VLM, VILA1.5-13B Lin et al. (2024), on a node equipped with eight NVIDIA A100 GPUs, each utilizing approximately 65 GB of memory. The training process takes about 30 hours to complete. We use an effective batch size of 256 and a learning rate of  $1 \times 10^{-5}$ . During fine-tuning, the entire model—including the vision encoder—is updated.

942

**B.2 LOW-LEVEL POLICY TRAINING DETAILS**

943

We train RVT2 (Goyal et al., 2024) and 3D-DA (Ke et al., 2024) as our lower-level policies. We keep overall architecture and training hyperparameters the same as paper settings. Specific details about how the inputs were modified other than the 2D path projection follow.

944  
945  
946  
947  
948  
949  
950  
951  
952

For low-level policy training, we train the policies on ground truth paths constructed by projecting trajectory end-effector points to the camera image. In order to also ensure the policies are robust to possible error introduced by HAMSTER VLM predictions during evaluation, we add a small amount of random noise ( $N(0, 0.01)$ ) to the 2D path  $(x, y)$  image points during training to obtain slightly noisy path drawings.

953  
954

**RVT2.** We remove the language instruction for RVT-2 when conditioning on HAMSTER 2D paths.

955  
956  
957

**3D-DA.** No changes such as removing language were performed for 3D-DA’s inputs as we saw a performance drop when removing language from the tasks.

958  
959  
960**C EXTENDED RESULTS**961  
962**C.1 VLM REAL WORLD GENERALIZATION STUDY**963  
964  
965  
966  
967

The full list of task descriptions for this study is below (see Section 5.3 for the main experiment details). Duplicates indicate different images for the same task. We plot some additional comparison examples in Figure 8. Note that the path drawing convention in images for this experiment differ from what is given to the lower-level policies as described in Section 4.2 as this multi-colored line is easier for human evaluators to see.

968  
969  
970  
971

1. screw in the light bulb on the lamp
2. screw in the light bulb on the lamp
3. screw in the light bulb on the lamp
4. screw out the light bulb and place it on the holder

972

973

974

975

976

977

978

979

980

981

982

983

984

985

986

987

988

989

990

991

**Inst:** Screw in the light bulb on the lamp



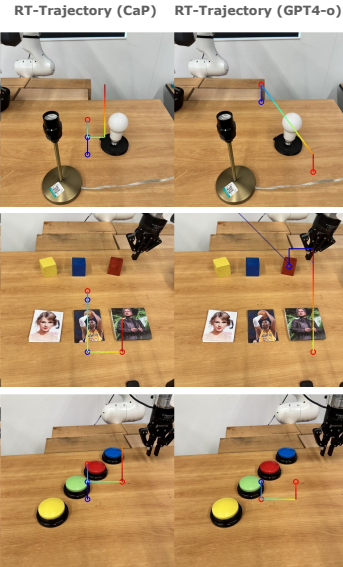
Hamster w/o Sim Data



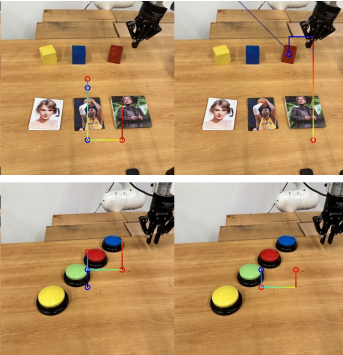
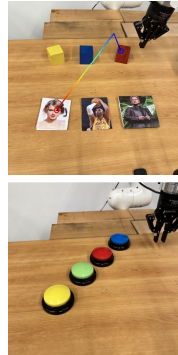
Hamster



RT-Trajectory (CaP)



**Inst:** Move the block on the right to Taylor Swift



**Inst:** Press the button with color of leaf, then press the button with color of banana



Figure 8: Human VLM evaluation example images and instructions along with corresponding trajectories from HAMSTER without any finetuning on (RLBench) simulation data, HAMSTER finetuned on all the data in Section 4.1, RT-Trajectory (Gu et al., 2023) with Code-as-Policies (Liang et al., 2023) powered by GPT-4o (Achiam et al., 2023), and RT-Trajectory powered by GPT-4o directly.

996

5. screw out the light bulb and place it on the holder
6. screw in the light bulb
7. screw in the light bulb on the lamp
8. move the blue block on Taylor Swift
9. pick up the left block and put it on Jensen Huang
10. move the block on the right to Taylor Swift
11. place the yellow block on Kobe
12. pick up the blue block and place it on Jensen Huang
13. move the red block to Kobe
14. press the button on the wall
15. press the button to open the left door
16. press the button to open the right door
17. open the middle drawer
18. open the bottom drawer
19. open the top drawer
20. open the middle drawer
21. open the bottom drawer
22. press the button
23. press the button
24. press the orange button
25. press the orange button with black base
26. press the button
27. pick up the SPAM and put it into the drawer
28. pick up the orange juice and put it behind the red box

- 1026        29. pick up the tomato soup and put it into the drawer  
1027        30. pick up the peach and put it into the drawer  
1028        31. move the mayo to the drawer  
1029        32. move the dessert to the drawer  
1030        33. pick up the object on the left and place it on the left  
1031        34. pick up the fruit on the left and put it on the plate  
1032        35. pick up the milk and put it on the plate  
1033        36. press the button with the color of cucumber, then press the button with color of fire  
1034        37. press the button with color of banana  
1035        38. press the button with color of leaf  
1036        39. press the button with color of leaf, then press the one with color of banana  
1037        40. press left button  
1038        41. pick up the left block on the bottom and stack it on the middle block on top  
1039        42. make I on top of C  
1040        43. put number 2 over number 5  
1041        44. stack block with lion over block with earth  
1042        45. pick up the left block on the bottom and stack it on the middle block on top  
1043        46. stack the leftest block on the rightest block  
1044        47. stack the block 25 over block L  
1045        48. put the left block on first stair  
1051  
1052  
1053  
1054  
1055  
1056  
1057  
1058  
1059  
1060  
1061  
1062  
1063  
1064  
1065  
1066  
1067  
1068  
1069  
1070  
1071  
1072  
1073  
1074  
1075  
1076  
1077  
1078  
1079